IOP Publishing Journal of Physics: Condensed Matter
J. Phys.: Condens. Matter **32** (2020) 255502 (13pp) https://doi.org/10.1088/1361-648X/ab7c16

Quantitative study of electronic whispering gallery modes in electrostatic-potential induced circular graphene junctions

T Lien Le[1] and V Lien Nguyen[2,3,4]

[1] University of Science and Technology of Hanoi, Vietnam Academy of Science and Technology, 18 Hoang Quoc Viet, Hanoi, Vietnam
[2] Institute for Bio-Medical Physics, 109A Pasteur, 710115 Hochiminh City, Vietnam
[3] Theoretical and Computational Physics Dept., Institute of Physics, VAST 10 Dao Tan, Ba Dinh Distr., 118011 Hanoi, Vietnam

E-mail: nvlien@iop.vast.ac.vn

Received 14 October 2019, revised 20 February 2020
Accepted for publication 3 March 2020
Published 25 March 2020

Abstract

Electronic whispering gallery modes (EWGMs) have been recently observed in several circular graphene junctions, pn and pp′, created in scanning tunneling microscopy experiments. By computing the local density of states within the Dirac–Weyl formalism for massless fermions we demonstrate that the EWGMs may really be emerged in any type of the electrostatic-potential induced circular graphene junctions, including uni-junctions (e.g. np- or pp′-junctions) as well as bipolar-junctions (e.g. pnp-heterojunctions). Surprisingly, quantitative analyses show that for all the EWGMs identified (regardless of junction types) the quality (Q) factors seem to be $\leq 10^2$, very small compared to those in ordinary optical whispering gallery modes microresonators, while the corresponding mode radii may tunably be in nanometer-scale. Our theoretical results are in good agreement with existent experimental data, putting a question to the application potential of the EWGMs identified.

Keywords: whispering gallery modes, graphene, circular junctions

(Some figures may appear in colour only in the online journal)

1. Introduction

The optical microresonators (or microcavities) that confine the light to small volumes by resonant recirculation are widely utilised in modern linear and nonlinear optics [1]. The most desirable resonators would confine light without loss and would have resonant frequencies defined precisely. In practice, optical resonators are characterised by the two parameters, the quality factor (Q-factor) and the mode volume (V), that respectively describe the temporal and spatial confinement of light in devices. Resonators with potential applications are those of high Q and small V. It appears that an extremely high value of Q may be achieved in the so-called whispering-gallery microresonators of very small volume [2–5]. In these microresonators, like dielectric microspheres, microdisks, or microtori, the light is effectively confined by repeated total internal reflections at the curved boundaries, giving rise to resonances. The circular optical modes emerged in such resonators are often referred to as whispering-gallery modes (WGMs). The Q-factor of optical WGMs may be as high as $\sim 10^{10}$, depending primarily on the resonator material and a perfection of dielectric surfaces [3]. With a very high Q in combination of other advantages such as very small mode volume and very simple geometry-structure, WGM-resonators emerged as the most potential optical resonators for a variety of applications [2, 3].

As well-known, there is a close similarity between light-rays in geometrical optics and ballistic trajectors of electrons. This similarity attracted much more attention by the

[4] Author to whom any correspondence should be addressed.

discovery of graphene, in which massless charge-carriers exhibit the photon-like linear dispersion and gain a very large mean-free path (of micrometer even at room temperature) [6]. It was established that the transport of electrons through an electrostatic potential barrier in a graphene heterostructure may well resemble the optical refraction at a surface of metamaterials with negative refractive index [7, 8]. As a consequence, the graphene np-junctions could be perfectly used to create an electronic analogue of the Veselago optical lens [7]. And, moreover, the scanning tunneling microscope (STM)-tip induced circular graphene np-junctions that are extensively exploited to study different properties of Dirac fermions confined by an axially symmetric electrostatic potential barrier [9–11] should act as electronic WGM-resonators in producing circular electronic modes analogous to the optical WGMs. Indeed, recently, electronic whispering-gallery modes (EWGMs) have been reported in several STM-experiments [12–14]. Owing to the dual-gate structure, the back-gate and top-gate, STM-based EWGM-resonators are fully tunable in the meaning that both the resonator size and the np-interface potential may be independently varied by changing suitably the back-gate voltage, the top-gate potential and the tip-to-graphene distance [14]. EWGMs in these resonators can be detected by measuring the tunneling differential conductance that features the local density of states (LDOSs) spectrum in dependence on the tip-sample bias, back-gate voltage, and spatial position (from the centre of the tip). So, the observed EWGMs can be theoretically understood by calculating the LDOS for the massless Dirac-like fermions under a suitable tip/gate-induced electrostatic potential. In the continuum calculation reported in [12] this potential is simply assumed to have the parabolic form, while in the tight-binding model used in [14] it is the Thomas–Fermi approximated potential. Both the studies have unambiguously confirmed an emergence of EWGM-spectra in STM-tip induced circular graphene resonators. Here, we note that all the studies in [12–14] concern the resonators with np/pn-junctions. Very recently, it was reported that similar EWGMs have been observed even in the STM-tip induced circular graphene resonator with pp′-junctions [15].

Actually, EWGMs are known as an almost periodic sequence of resonances emerged in an energy spectrum of a resonator. For the circular graphene resonators under study, these resonances truly describe the quasi-bound states (QBSs) that are formed as a result of interference processes of the electronic waves, undergone multiple Klein-scatterings by the electrostatic confinement potential on the inside of the resonator [16]. Generally, QBSs could be created by any electrostatic confinement potentials [16, 17]. The structure of QBS-spectra however depends on the interference pattern of wave functions inside the resonator, and the later, in turn, is highly sensitive to the characteristics of the confinement potential (such as its magnitudes, signs or sizes). Also, these characteristics are closely correlated with each other in affecting the QBS-spectra. So, it seems that to create a QBS-spectrum with EWGMs in an electrostatic-potential induced circular graphene resonator of any junction-type one has just to set the appropriate characteristics to the confinement potential. And, in principle, EWGMs may emerge in any type of these junctions, though the chance of getting them as well as their quality, i.e. Q-factor and mode volume V, might be different, depending on the junction type. Since these quantities, Q and V, are primary characteristics of EWGMs, one certainly has to determine them first in examining EWGM-spectra.

The purpose of the present theoretical work is to quantitatively study the EWGMs emerged in various models of circular graphene junctions, including uni-junctions such as np-junctions (CGNPJs) or pp′-junctions (CGPP′Js) and bipolar-junctions such as pnp-heterojunctions (CGPNPHJs). The junctions are assumed to be created by axially symmetric electrostatic potentials like those in STM-experiments. The study was carried out within the framework of the Dirac–Weyl formalism for massless fermions in the presence of the suggested confinement potential. For each of these resonator-models we searched for EWGMs by analysing the LDOSs calculated in wide value-ranges of confinement-potential parameters. For all the identified EWGMs we evaluated the Q-factors and the effective mode radii[5], following the way that is often used for optical WGM-resonators. Qualitatively, our studies demonstrate that the EWGMs may emerge in electrostatic-potential induced circular graphene resonators with any type of junctions, depending primarily on the confinement potential parameters. Quantitative analyses show that for all the EWGMs identified the Q-factors seem always to be $\leqslant 10^2$, very small compared to those in ordinary optical WGM-microresonators (of $\simeq 10^5$–10^8 [1, 3]), while the corresponding mode radii may tunably be in nanometer-scale. Our theoretical results are in a good agreement with existent experimental data [12, 14, 15], putting a question to the application potential of the EWGM identified.

Thus, we are interested in the circular graphene junctions created by an axially symmetric electrostatic confinement-potential $U(r)$ in a continuous single-layer graphene sheet. Neglecting the valley scattering and using the units such that $\hbar = 1$ and the Fermi velocity $v_{\mathrm{F}} = 1$, the low-energy electronic excitations in these structures can be described by the two-dimensional (2D) massless Dirac–Weyl Hamiltonian:

$$\mathcal{H} = \vec{\sigma}\vec{p} + U(r), \tag{1}$$

where $\vec{\sigma} = (\sigma_x, \sigma_y)$ the Pauli matrices and $\vec{p} = -\mathrm{i}(\partial_x, \partial_y)$ the 2D momentum operator. In STM-experiments the potential $U(r)$ is mainly resultant from a combined effect of the tip-sample potential and the back-gate voltage.

Given $U(r)$, we computed LDOSs for the studied resonator, using the approach suggested in [18, 19]. For practical purposes, the computing procedure is summed up in the appendix A. Resulted quantities of interest are as follows: (a) the LDOSs counted for a given total angular momentum j, the partial LDOSs, $\rho^{(j)}(E, r)$ (A3) that depend on the energy E, distance r and momentum j; (b) the LDOS $\rho(E, r)$ (A2) that is the sum

[5] There are different definitions of the mode volume for optical WGM-resonators, depending on the problem of interest [2]. Here, instead, we are interested in the mode radius that is entirely definite and may be used to calculate, for instance, the mode area in 2D-resonators [2].

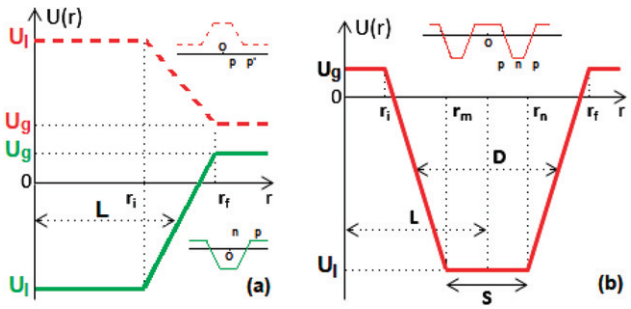

Figure 1. Models of radial electrostatic potentials $U(r)$ that create the two types of circular graphene junctions under study: (a) Uni-junctions: green-solid profile—CGNPJs and red-dashed profile—CGPP′Js with average radius L and (b) Bipolar-junctions: red-solid profile—CGPNPJs with average radius L and average width D. All the modelled potentials are constant at the limiting distances of $r \leqslant r_i$ and $r \geqslant r_f$.

of partial LDOSs over all possible j; and (c) the total density of states (TDOS) $\rho_{\rm T}(E)$ (A8) that is determined by integrating $\rho(E, r)$ over r. All the features of a resonance spectrum are definitely manifested in its LDOS and TDOS. Certainly, no all junction-samples may reveal EWGMs. So, we had to search for these modes, varying different confinement-potential parameters. Qualitatively, EWGMs can be identified as a spectrum with an almost periodic sequence of resonances, appearing in a narrow range of energy in one side and close to the charge neutrality point, while in the other side the spectrum shows itself to be featureless [14].

Once a EWGM-spectrum is identified we have quantitatively examined each of most profound resonances in the spectrum by evaluating its partial quality-factor Q_i and partial mode radius R_i[5]. To this end, for the resonance at energy E_i, we measure the resonance width δE_i (by fitting resonance peak into an appropriate Lorentzian profile) and the resonance spacing ΔE_i (see figure 6(d)). Quantities Q_i and R_i could be then determined in the way as that used for optical WGM-resonators: $Q_i = \omega_i \tau_i \equiv |E_i|/\delta E_i$ and $R_i \approx \hbar v_{\rm F}/\Delta E_i$, where $\omega_i = |E_i|/\hbar$ is the resonant-mode frequency and $\tau_i = \hbar/2\delta E_i$ is the lifetime of the mode ($\hbar =$ Planck constant$/2\pi$ and $v_{\rm F} \approx 10^6 \mathrm{m\,s^{-1}}$ is the Fermi velocity) [3, 4, 12]. From partial quantities $[Q_i]$, $[R_i]$ and $[\Delta E_i]$ we respectively deduced the average quantities Q, R and Δ which could be used to characterise the examined EWGM-spectrum on the whole. Such studies have been realised for all the EWGM-spectra identified in circular graphene resonators with different junctions types, uni-junctions CGNPJs and CGPP′Js as well as bipolar-junctions CGPNPHJs.

Thus, first we have to define radial confinement potentials $U(r)$. For the resonators with uni-junctions, the potential $U(r)$ is chosen in the form (see figure 1(a)):

$$U(r) = \begin{cases} U_l & \text{for } r \leq r_i \\ U_l + \dfrac{r - r_i}{r_f - r_i}(U_g - U_l) & \text{for } r_i < r < r_f \\ U_g & \text{for } r \geq r_f. \end{cases} \tag{2}$$

The distances r_i and r_f in this equation can be merely expressed as $r_i = (1 - \alpha)L$ and $r_f = (1 + \alpha)L$, where the quantity α with $0 \leq \alpha \leq 1$ and the length L respectively measure the smoothness of the junction–boundary potential and the average radius of the junction (see figure 1(a)). So, the potential $U(r)$ suggested in equation (2) is entirely characterised by the four parameters: U_l, U_g, L, and α. In relation to the STM-experiments, the potentials U_g and U_l should be thought of as defined respectively by the back-gate voltage and the tip-sample and back-gate voltages combined, while the two other parameters, L and α, are essentially related to the tip size and the tip-sample distance [14]. The potential $U(r)$ of equation (2) is quite general, describing all possible circular graphene uni-junctions. Particularly, this potential $U(r)$ describes CGNPJs if $U_l < 0$ and $U_g > 0$. In the other case, when both U_l and U_g are positive, it describes CGPP′Js. Here, it is useful to note that due to the electron-hole symmetry in the model under study a simultaneous change in sign of the two potentials U_l and U_g as well as the energy E does not make the spectrum changed. So, we should consider only two types of uni-junctions, e.g. CGNPJs and CGPP′Js. Certainly, this note should also be applied to the bipolar-junctions introduced below.

In order to model the circular graphene bipolar-junctions, i.e. npn- or pnp-heterojunctions, we define the radial confinement potential $U(r)$ as (see figure 1(b)).

$$U(r) = \begin{cases} U_g & \text{for } r \leq r_i \\ U_g + \dfrac{r - r_i}{r_m - r_i}(U_l - U_g) & \text{for } r_i \leq r \leq r_m \\ U_l & \text{for } r_m < r < r_n \\ U_l - \dfrac{r - r_n}{r_f - r_n}(U_l - U_g) & \text{for } r_n \leq r \leq r_f \\ U_g & \text{for } r \geq r_f. \end{cases} \tag{3}$$

Actually, the labelled distances $(r_\nu, \nu = i, m, n, f)$ in this expression can be expressed as $r_i = L - D + S/2, r_m = L - S/2, r_n = L + S/2$ and $r_f = L + D - S/2$, where L, D, and S may be effectively understood as the average radius of junction, its average width and the tip/top-gate size, respectively (see figure 1(b)). Thus, in the model suggested a circular graphene bipolar junction is characterised by the five parameters: U_l, U_g, L, D, and S. The potentials U_l and U_g could be here thought of as having the same source as those in the potential of equation (2). In addition, to describe bipolar-junctions these two potentials must be different in sign, $U_l U_g < 0$, implying the two possible cases of sign-realisations. However, as noted above on the electron-hole symmetry, we need consider only one of these cases, e.g. the case of $U_l < 0$ and $U_g > 0$ (i.e. CGPNPHJs in figure 1(b)). Note that an equal smoothness is explicitly introduced at both heterojunction boundaries in the potential $U(r)$ of equation (3).

Importantly, both the potentials in equations (2) and (3) become constant in the two limits of small and large distances, $r \leq r_i$ and $r \geq r_f$ (see figure 1(a) and (b)), that would significantly facilitate the LDOS-computations [19]. In particular case of $U_g \equiv 0$, these potentials $U(r)$, equation (2) as well as equation (3), seem to have the ordinary trapezoidal profiles.

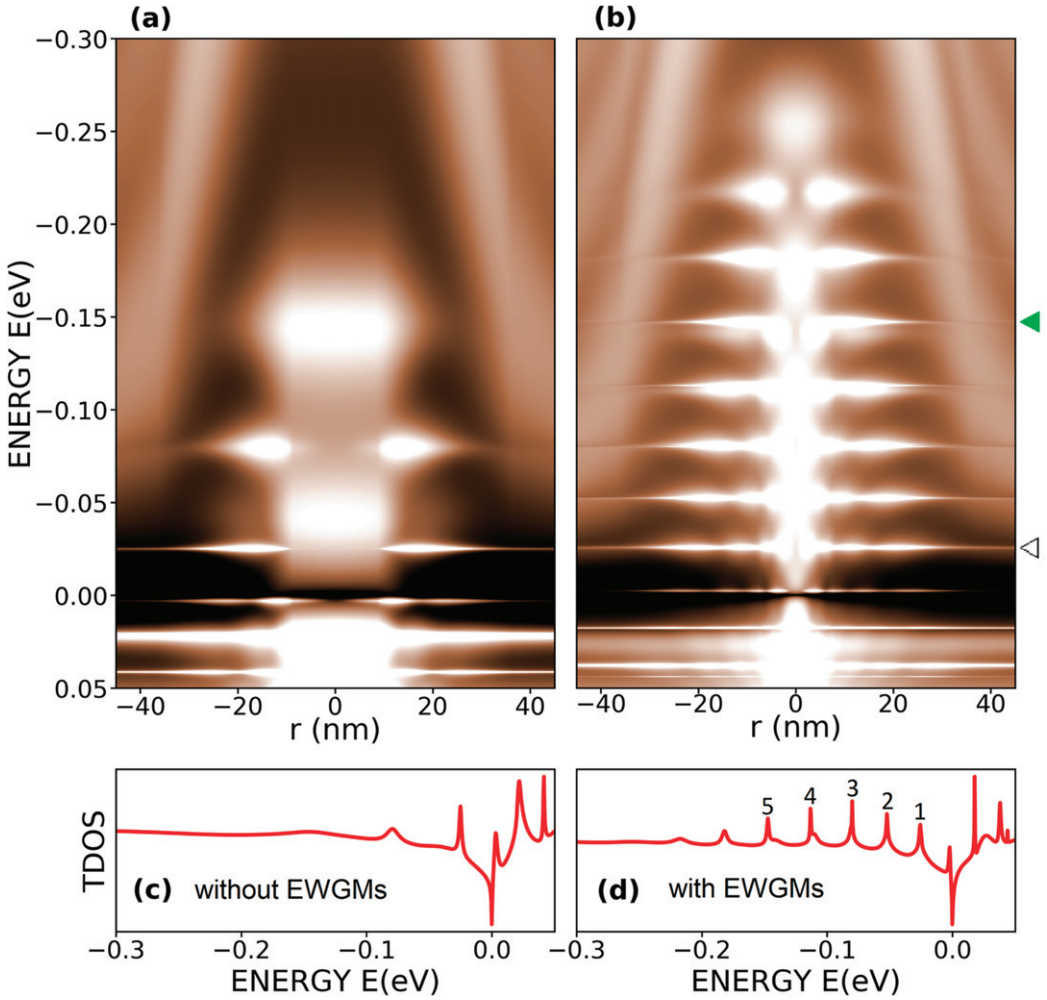

Figure 2. (a) Map of LDOS as a function of distance r and (c) corresponding TDOS (in arbitrary unit) for the CGNPJ with potential parameters $[U_l, U_g, L, \alpha] = [-0.35\,\text{eV}, 0.02\,\text{eV}, 15\,\text{nm}, 0.9]$. (b) and (d) are the same as (a) and (c), respectively, but for another CGNPJ with $[U_l, U_g, L, \alpha] = [-0.35\,\text{eV}, 0.02\,\text{eV}, 30\,\text{nm}, 0.5]$. While the spectrum in (a) and (c) is featureless, that in (b) and (d) clearly shows EWGMs.

The trapezoidal potentials are often used to describe the gate-induced graphene structures [20, 21], which are also referred to as circular graphene quantum dots [16, 18] or quantum rings [22, 23]. In reality, the trapezoidal shape is quite a good fit of the Lorentzian shape that is widely believed to be the profile of electrostatic potentials induced by a STM-tip [24]. An advantage of the potentials of equations (2) and (3) also lies in their simplicity so that the Hamiltonian of equation (1) could be exactly solved [18, 21].

So, given parameters of the potential $U(r)$ of equation (2) or equation (3), as mentioned above, we solved the eigenvalue equation for the Hamiltonian of equation (1), computed the LDOSs, searched for EWGM-spectra, and quantitatively analysed the EWGMs identified. Searching for EWGMs requires a bit of patience, though some guesses can be made, using experimental data for uni-junctions (for CGNPJs [14] and for CGPP′Js [15]). Anyway, we were able undoubtedly to identify the EWGMs in resonators with any type of junctions under study. In the case of uni-junctions, identified EWGMs resemble well existent experimental data. Below, in figures 2–5 we present the computational results for the CGNPJs, CGPP′J, and CGPNPHJ, respectively. These figures have the same structure, showing the qualitative behavior and quantitative characters of the EWGM examined. So, avoiding an unnecessary repeat, most detailed discussions relating to the CGNPJ in figures 2 and 3 may also be applied to the CGPP′J in figure 4 as well as the CGPNPHJ in figure 5.

Figure 2 presents the computed maps of LDOSs as a function of distance r (boxes (a) and (b)) and corresponding TDOSs (boxes (c) and (d)) for the two CGNPJs with different parameter values of the potential of equation (2) (given in the caption to the figure). Indeed, both the spectra in (c) and (d) show the resonances (or QBSs) which however carry very different features. The spectrum in box (c) is featureless, showing no particular relation between the magnitudes as well as the positions of emerged resonances (here, one might think of the so-called atomic collapse resonances [25]). On the contrary, the spectrum in box (d) shows an almost periodic sequence of resonances, appeared on one energy-side from the neutral point. This is the typical feature of EWGMs. To ensure that

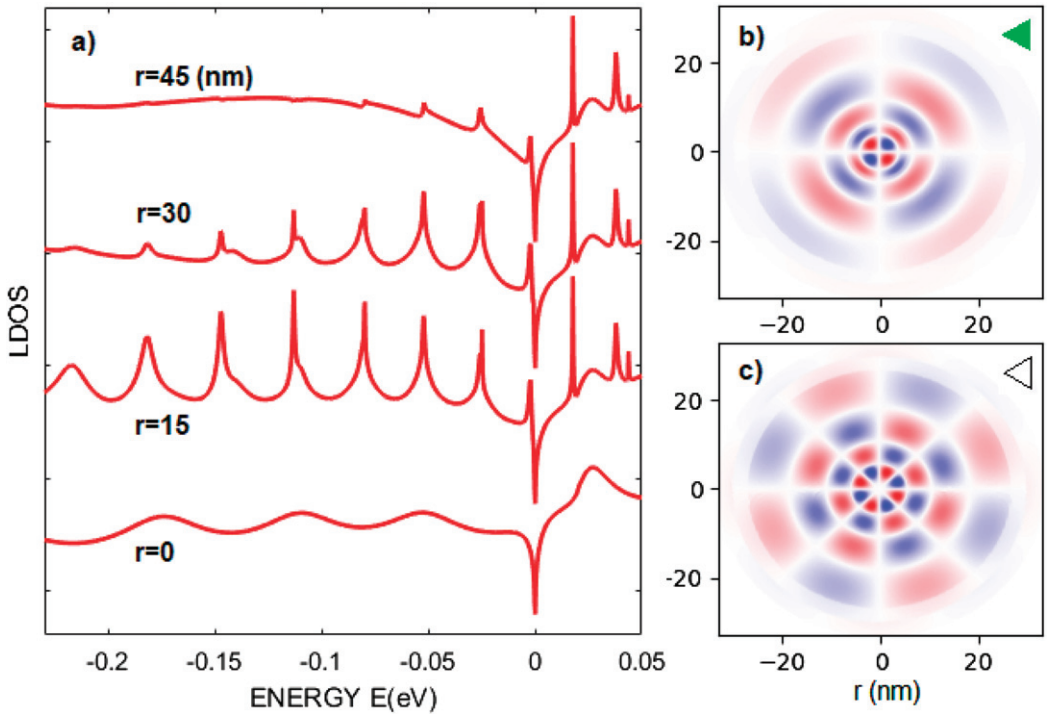

Figure 3. (a) LDOSs(E) taken from LDOS(E, r) in figure 2(b) at different distances r given in the figure; (b) spatial distributions of the LDOS for the two resonances/QBSs indicated respectively by the arrows in figure 2(b) [j = 1/2(7/2) for the lower (higher) state].

the LDOS in figure 2(b) really manifests a EWGM-spectrum we should further explore it.

In figure 3(a) we specifically display the LDOS(E), taken from LDOS(E, r) in figure 2(b) at different distances r, given in the figure. Note that for the CGNPJ-sample studied in this figure the junction–boundary region ranges from $r_i = 15$ nm to $r_f = 45$ nm. Correspondingly, as clearly seen from figure 3(a), the resonances mainly appear in the indicated region of the junction. In other words, electronic waves are mainly confined at the junction–boundary region, manifesting a characteristic feature of the EWGM-confinement. A similar conclusion can also be deduced from figure 3(b), where the spatial distributions of the LDOS are plotted for the two resonances/QBSs marked by the corresponding arrows in figure 2(b)[6]. The observed ring structure of these distributions is one more manifestation of the EWGM-confinement. Additionally, noting on a difference in the momentum j between these two QBSs, $j = 1/2(7/2)$ for the lower (higher) level in figure 2(b), we notice that with increasing j the confinement becomes stronger and the electronic wave functions become more localised near the junction boundary. This is in full agreement with the ordinary WGM-idea.

Thus, the TDOS in figure 2(d) indeed shows itself to be a EWGM-spectrum. To quantitatively evaluate this spectrum we measured the resonance energies E_i, resonance widths δE_i and resonance spacings ΔE_i for the five most profound resonances labelled by the numbers ($i = 1$–5) in the spectrum. Then we calculated the partial quality-factors [Q_i] and mode radii [R_i]. Obtained results are as follows: Q_i(eV) ≈ 14.23, 34.16, 61.40, 92.34, 78.40 and R_i(nm) ≈ 37.56, 36.83, 32.81, 29.73, 29.12 as $i = 1$–5. From these data we deduced the average values that characterise the whole EWGM-spectrum in figure 2(d): the quality factor $Q \approx 47.37$ and the mode radius, $R \approx 31.83$. Also, the resonance spacing ΔE_i seems to slightly increase from 27 meV to 34 meV as i increases from 1–5 with the average value of $\Delta \approx 31$ meV. These obtained values of the mode-radius $R \approx 32$ nm and the resonance spacing $\Delta \approx 31$ meV seem to be rather reasonable in relation to the junction size (average radius $L = 30$ nm). Here, as a reference, we would like to mention that the values $R \approx 50$ nm and $\Delta \approx 40$ meV have been reported for the experimental data from figure 2A in [12]. Concerning the Q-factor, however, the obtained value $Q \approx 45$ shows a complete surprise, it is too small compared to Q-factors in ordinary optical WGM-microresonators (≈ 10^5–10^8 [1, 3]). Regretfully, the Q-factor is not claimed in [12] as well as in the other experiment, relating to the EWGMs in CGNPJs [14]. So, we tried ourselves to get some rough estimations from the experimental data published. Analysing the three most profound resonances labelled 1′, 2′, and 3′ from figure 2D in [12] as well as the most profound resonances from figure 3g in [14], using the same way as described above, we learn that for all these experimental resonances the partial Q-factors are in the same order of value as the computing Q-factors presented above.

Next, we present in figures 4 and 5 the computing spectra obtained for a CGPP′J and CGPNPHJ, respectively. It should

[6] Figures 3(b), 4(d) and 5(d) have been drawn in the way as used for similar figures in [12]: the real part of the second spinor component of the Hamiltonian (1) is plotted for indicated resonances.

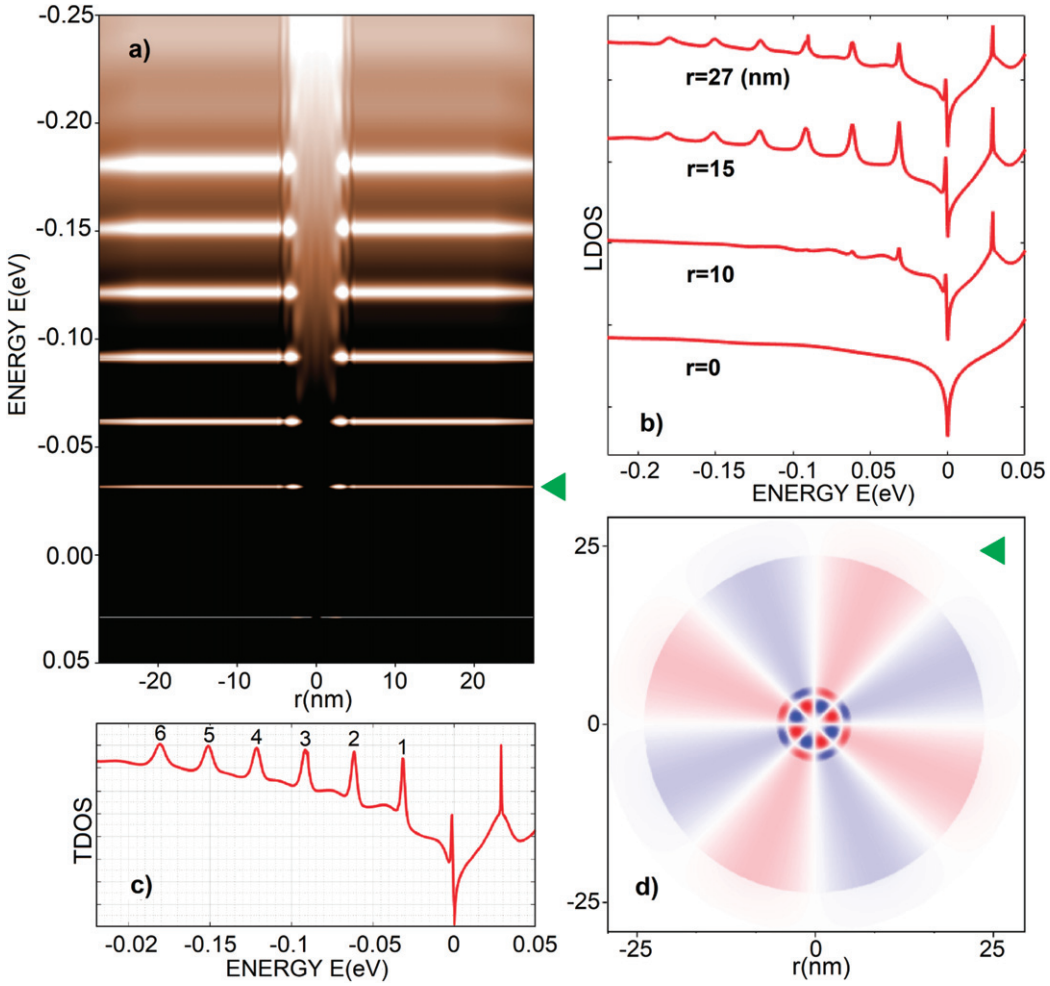

Figure 4. (a), (b), (c), and (d) are respectively the same as figures 2(b), 3(a), 2(d) and 3(b), but for the CGPP′J with potential parameters: $[U_l, U_g, L, \alpha] = [0.28\,\text{eV}, 0.06\,\text{eV}, 25\,\text{nm}, 0.0]$—step junction–boundary potential.

be again noted that each of figures 4 and 5 is very similar in both content and structure to figures 2(b)–(d) plus figure 3. So, we would like immediately to remark that, like figures 2 and 3 for the CGNPJ, figure 4 (or figure 5) qualitatively demonstrates an emergence of EWGMs in the CGPP′J (or CGPNPHJ) under study. Note that in accord with the experimental pp′-junction measured in [15] we have chosen the particular sample with a step junction–boundary potential for the first attempt to study EWGMs in CGPP′Js (in figure 1(a), step junction–boundary potentials are described by the dashed/solid lines with $x_i \equiv x_f$). And, this is the case reported in figure 4 (with potential parameters given in the figure).

Quantitatively, analyzing the six most profound resonances labelled by the numbers from 1–6 in the TDOS in figure 4(c), we obtained for the studied CGPP′J the partial Q-factors and mode radii as follows: (a) $Q_i \approx 16.09, 45.39, 18.18, 17.49, 16.56$ and 15.74 and (b) $R_i(\text{nm}) \approx 32.49, 33.30, 33.86, 33.58, 33.72$ and 33.86 as $i = 1$–6. So, on the whole, the studied CGPP′J is characterised by the average quality-factor of $Q \approx 21.57$ and mode radius of $R \approx 33.47$ nm. Correspondingly, for the resonance spacing that slightly decreases from 31 to 29.7 meV we have the average value $\Delta \approx 30$ meV. Analogously, for the six resonances numbered in the TDOS presented in figure 5(c) we obtained for the studied CGPNPHJ (as $i = 1$–6): (a) $Q_i \approx 21.38, 48.53, 40.23, 82.10, 54.64$ and 67.18 with the average value $Q \approx 46.47$; (b) $R_i(\text{nm}) \approx 39.92, 39.64, 38.31, 37.56, 36.36$ and 35.90 with the average mode radius $R \approx 37.51$ nm; and (c) the average resonance spacing $\Delta \approx 27$ meV. Overall, obtained values of R and Δ are rather reasonable in relation to the potential parameters of the studied junctions. We would here mention that for the CGPP′J measured in the experiment [15] the average level spacing was reported to be 48 meV. Concerning the Q-factors, however, the values obtained for both the CGPP′J in figure 4 and CGPNPHJ in figure 5 are very small, in the same order of value as those for CGNPJs analysed in figures 2 and 3.

Thus, it seems that all the three EWGM-spectra presented in figures 2–5 for circular graphene resonators of different junction-types show very small values of their Q-factors. A question may then be arisen about if such the small Q-factors are a particular property of the junctions studied. So, we largely searched for EWGMs, varying parameter values of the potential $U(r)$ for each junction type. As a brief summary, we present in figure 6 the TDOSs with EWGMs for three resonators of

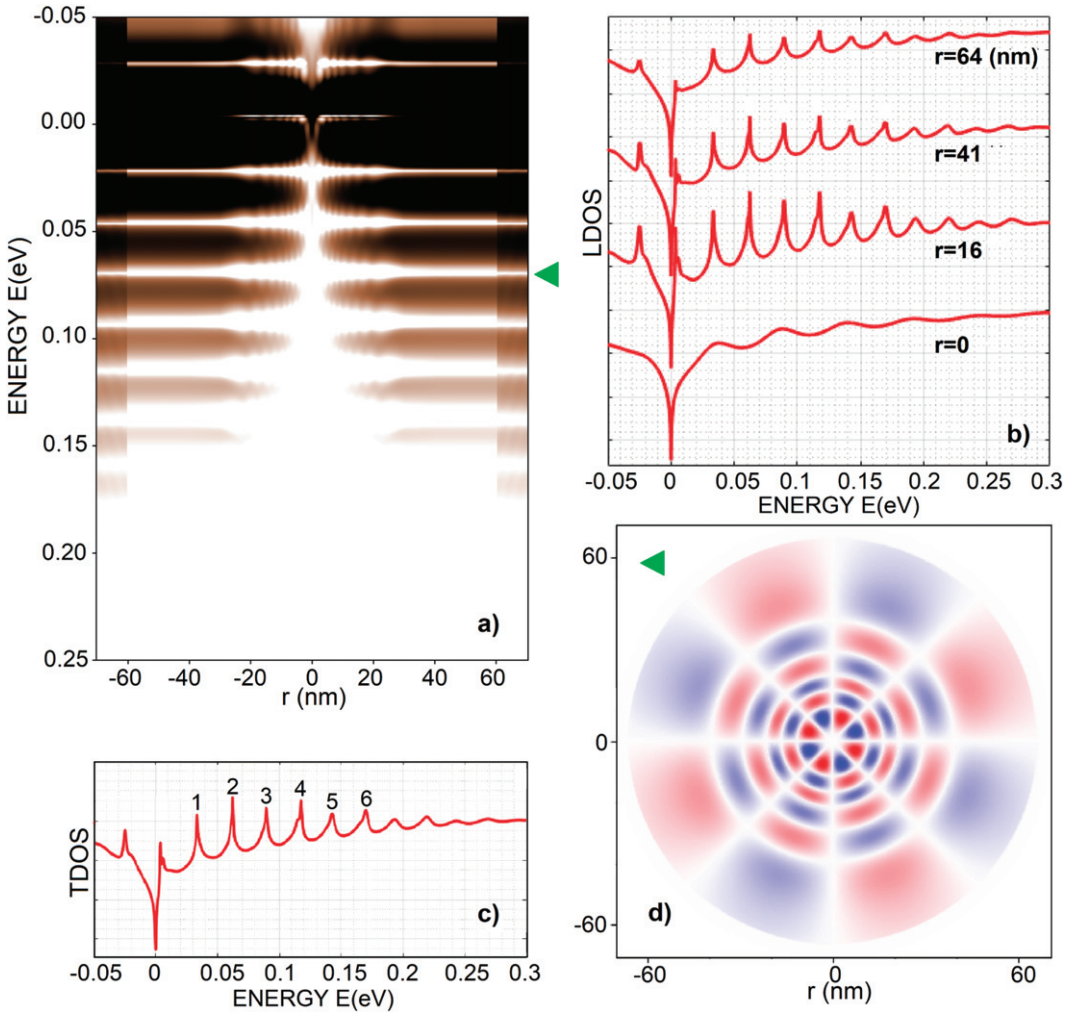

Figure 5. (a), (b), (c), and (d) are respectively the same as figures 2(b), 3(a), 2(d) and 3(b), but for the CGPNPHJ with potential parameters: $[U_l, U_g, L, D, S] = [-0.60\,\text{eV}, 0.15\,\text{eV}, 40\,\text{nm}, 25\,\text{nm}, 2\,\text{nm}]$.

each junction type: (a) CGNPJs; (b) CGPP′Js, and (c) CGPNPHJs (with potential-parameter values given in the figure). Obviously, all these TDOSs show the EWGMs, similar to the TDOSs in figures 2(a), 4(c) and 5(c). Note that some of these TDOSs are specially collected from the junctions with step junction–boundary potential (in the case of CGPNPHJs, it means $x_i \equiv x_m$ and $x_n \equiv x_f$, see figure 1(b)).

Quantitative analyses of all the EWGM-spectra shown in figure 6 are in detail given in tables B1 and B2 (appendix B). As can be seen in table B2, the values of mode radii R and resonance spacings Δ obtained for all the examined resonators, (s1)–(s9) (each with five numbered resonances—see figure 6(a)–(c)), vary from ≈ 14 to ≈ 67 nm and from ≈ 15 to ≈ 69 meV, respectively. These values of R and Δ are in the same order of value as the corresponding data reported in figures 2–5 and seem rather reasonable, depending on the resonator size. As for the quality factors, though the three CGPNPHJs, (s7)–(s9), show somewhat improved values of Q, about a 100, totally, for all examined resonators, the Q-factors are still small, $\leqslant 10^2$. We would like here to emphasise that such the Q-factors are found in the EWGMs emerged in all the electrostatic-potential induced circular graphene junctions under study, regardless of the junction type as well as the smoothness of junction–boundary potentials.

Lastly, we would clarify in figure 6(d) the way we have used to evaluate the EWGM-characteristics. For the resonance (or QBS) of interest (for instance, the resonance marked by the arrow in the last curve in figure 6(b)) the quantities to be determined are as follows: (a) the resonance energy E_i that appears as the eigenvalue of the Dirac equation, (b) the resonance width δE_i that is determined by fitting the resonant peak (dashed line) to an appropriate Lorentzian profile (solid line), following the standard way of evaluating this quantity (see, for example, [26]), and the resonance spacing ΔE_i that is determined as shown in figure 6(d). The quantities E_i and δE_i are then used to evaluate partial Q_i and R_i as described above.

Thus, we have theoretically studied the EWGMs emerged in energy spectra of electrostatic-potential induced circular graphene junctions, including all types of uni-junctions as well as bipolar-junctions. To this end, we modelled the studied junctions by appropriate electrostatic confinement potentials and calculated the LDOSs of structures within the framework

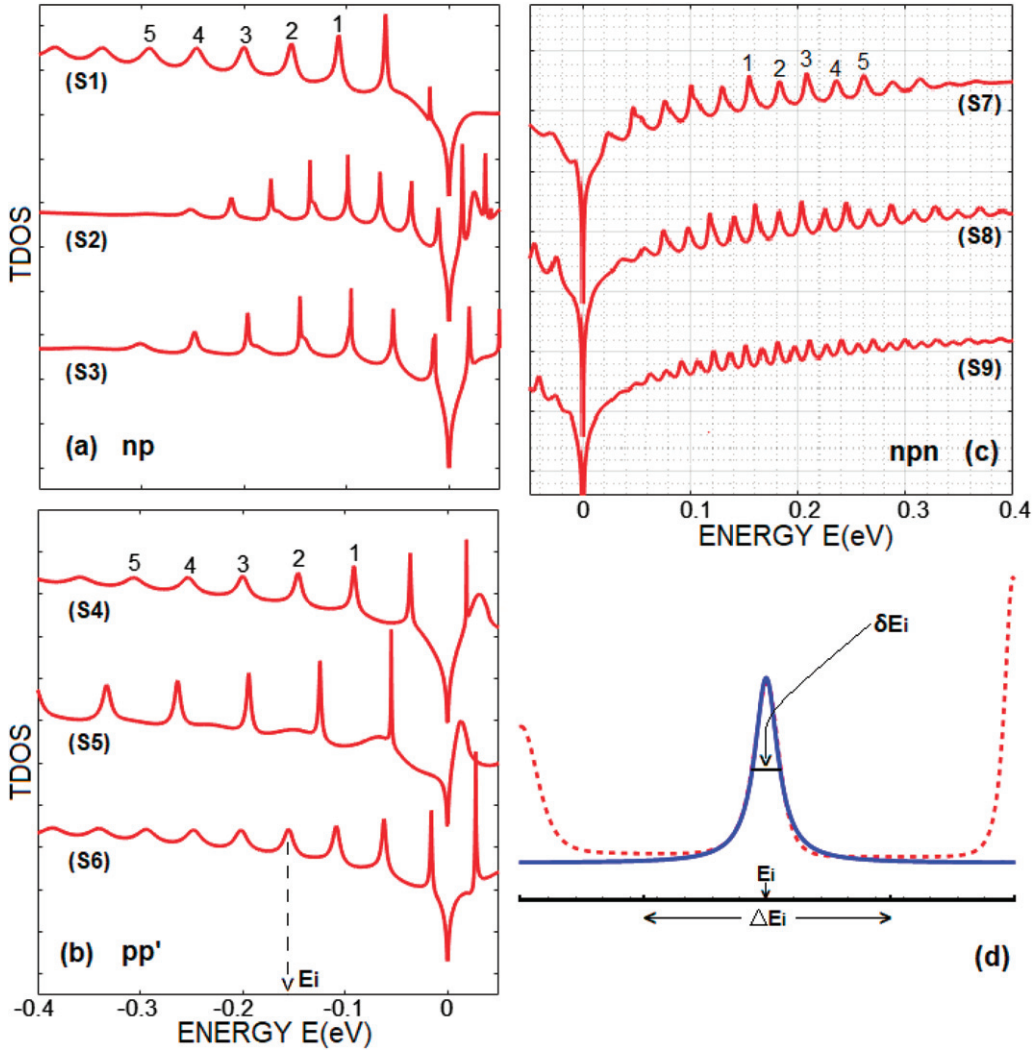

Figure 6. The TDOSs are shown for: (a) three CGNPJs with potential parameters $[U_l(\text{eV}), U_g(\text{eV}), L(\text{nm}), \alpha] =$ (s1) $[0.15, -0.02, 15, 0.0]$, (s2) $[-0.4, 0.02, 27, 0.5]$ and (s3) $[-0.5, 0.05, 20, 0.5]$; (b) three CGPP′Js with potential parameters $[U_l(\text{eV}), U_g(\text{eV}), L(\text{nm}), \alpha] =$ (s4) $[0.28, 0.04, 13, 0.2]$, (s5) $[0.35, 0.02, 10, 0.0]$ and (s6) $[0.2, 0.02, 15, 0.1]$; and (c) three CGPNPHJs with potential parameters $[U_l(\text{eV}), U_g(\text{eV}), L(\text{nm}), D(\text{nm}), S(\text{nm})] =$ (s7) $[-0.6, 0.15, 40, 8, 8]$, (s8) $[-0.7, 0.3, 50, 15, 2]$ and (s9) $[-0.7, 0.3, 70, 15, 2]$. (d) Demonstration of the method used to evaluate the partial ΔE_i and δE_i for the resonance at energy E_i (indicated by the arrow from the lowest curve in figure 6(c): the resonance peak (red-dashed) is fitted to the appropriate Lorentzian profile (solid-blue)

of the Dirac–Weyl formalism for massless fermions. Calculations have been carried out for many junction-samples of each junction-type, varying potential-parameter values. From obtained LDOSs we identified those with EWGMs, following the way of identifying the optical WGMs. Remarkably, our study shows that EWGMs could be emerged in energy spectra of circular graphene resonators with any junction-type, uni-junctions or bipolar junctions, including those with a step junction–boundary potential. Further, for all the identified EWGMs we evaluated their characteristics such as the Q-factors, mode radii R, and resonance spacings Δ. Obtained values of R and Δ are rather reasonable, depending on the potential parameters. However, obtained Q-factors seem always to be very small (generally, $\leqslant 10^2$), compared to those in ordinary optical WGM-microresonators. Though all these theoretical results describe rather well the existent experimental data, such the small values of Q cause a surprise.

For optical WGM-resonators the Q factor is limited by the losses due to radiation/tunnel, material attenuation or scattering by geometrical imperfections. The radiative loss is related to the fact that unlike a flat surface the total internal reflection from a curved surface does not exist, so it is unavoidable for any resonators of finite radius. Actually, an increase of resonator radius may very strongly enhance the Q factor. Unfortunately, this simultaneously results in unwanted consequences such as a large mode volume or an un-equidistant spectrum that seriously affect application potentials of the device. In practice, for each kind of resonator there exists optimum sizes to be chosen, depending on the light wavelength λ. Generally, the resonator radius should be much larger than λ. Quality factor $Q \approx 8 \times 10^9$ at $\lambda = 800\,\text{nm}$ was reported for the silica sphere with radius of 400 μm [2]. Optimum radii of droplets in liquid WGM-resonators are often much smaller, $\sim 20\,\mu\text{m}$, while for some crystalline resonators they may be as large as

few milimeters [3]. Similarly, for large mode indices while the radiative loss may be diminished strongly, other losses become important, resulting in unwanted spectra. So, the typical index of modes should be optimally determined, depending on material, light-wavelength and resonator size. Ideally, in spherical resonators with large radius the WGMs of high indices are strongly confined to the cavity 'equatorial' region so effective WGM-volume occupies only a small fraction of the total sphere volume. In practice, the confinement picture of WGMs essentially depends on the chosen resonator size and mode index.

In crucial difference from ordinary WGM-resonators in optics that are fabricated with sharp boundaries, the EWGM-resonators under study are based on graphene and bounded by electrostatic potentials. As is well-known, due to Klein tunneling these potentials cannot strictly confine Dirac-like electrons in circular resonators except for the particular state of zero energy [24, 27]. This situation sustains as the resonator radius increases. In the limit of large resonators, when confinement potentials become one-dimensional, there is still no total reflection (as shown in [28] for rectangular potentials and in [21] for trapezoidal ones). Moreover, our computations demonstrate that within the framework of modelled confinement potentials there are fewer chances of realizing EWGMs in larger resonators (see the appendix C). Actually, a magnetic field might enhance an electron localisation in the circular resonators, but it also induces weak resonances, destroying the EWGM-feature of spectra [15]. Alternatively, it was also shown that in the limit of one-dimensional potentials a total reflection might be realized by tuning a strong Rashba spin–orbit coupling [29] that, however, like magnetic fields, does not support the EWGMs of interest. Electrostatic potentials have a great advantage of that they could be externally controlled. However, with respect to the EWGMs these potentials have a key weakness of that they cannot completely suppress the Klein tunneling, causing a diminution of Q-factors. So, we assume that a smallness of Q-factors is an inherent character of all circular graphene resonators created by electrostatic potentials. Perhaps, this unwanted effect of Klein tunneling might be partly reduced, for example, by using a system of several concentric radial potential barriers in the way similar to the system of dielectric rings suggested in [5] for optical resonators.

Acknowledgments

We are very grateful to H Chau Nguyen for helpful discussions. We also thank T T Nhung Nguyen, T D Linh Dinh and H Minh Lam for some collaboration in the first step of numerical computations. This work is funded by Vietnam National Foundation for Science and Technology Development (NAFOSTED) under Grant No. 103.02-2015.48.

Appendix A. Computations of LDOSs and TDOSs

Both the potential models $U(r)$ (2) and (3) have the two typical properties: (a) they are axially symmetric and (b) become constant in the limits of small r ($U(r) \equiv U_i$ at $r \leqslant r_i$) and large r ($U(r) \equiv U_f$ at $r \geqslant r_f$). The computing procedure realised below can be applied to all the potentials $U(r)$ with these properties [16, 19].

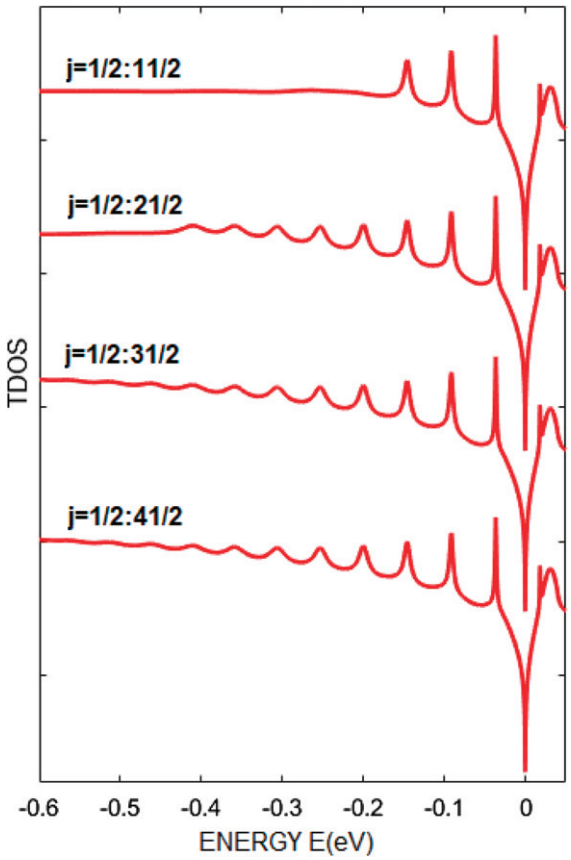

Figure A1. The TDOSs calculated from the LDOSs (A2) with $j_{\max}$, increasing from $11/2$ (top curve) to $41/2$ (bottom curve), are shown to demonstrate that the summation over j in LDOS of equation (A2) may rightly be truncated at $j_{\max} = 31/2$ for this sample: the two lower curves with $j_{\max} = 31/2$ and $41/2$ in the figure are practically the same. Data shown here are for the CGNPJ with the LDOS and TDOS presented in figures 2(b) and (d), respectively.

Due to an axial symmetry of $U(r)$, in the polar coordinates (r, ϕ), the eigenfunctions associated with the eigenvalues E of the Hamiltonian (1) can always be found in the form $\Psi_j(E, r, \phi) = \mathrm{e}^{ij\phi}(\mathrm{e}^{-i\phi/2}\chi_j^{(A)}(E, r), \mathrm{e}^{+i\phi/2}\chi_j^{(B)}(E, r))^T$, where the total angular momentum j takes half-integer values and $\chi_j^{(A/B)}(E, r)$ are the partial radial wavefunctions on the graphene A/B-sublattices. The radial wavefunction $\chi_j(E, r) = (\chi_j^{(A)}(E, r), \chi_j^{(B)}(E, r))^T$ obeys the equation

$$\mathrm{i}\frac{\partial \chi_j(E, r)}{\partial r} = \mathcal{H}(r)\chi_j(E, r), \tag{A1}$$

where the formal radial Hamiltonian $\mathcal{H}(r)$ is defined by

$$\mathcal{H}(r) = \begin{pmatrix} \mathrm{i}\dfrac{j - 1/2}{r} & U(r) - E \\ U(r) - E & -\mathrm{i}\dfrac{j + 1/2}{r} \end{pmatrix}.$$

The LDOS can be defined as

$$\rho(E,r) = \sum_{j=-\infty}^{+\infty} \rho^{(j)}(E,r) \tag{A2}$$

with the partial LDOS for the j-momentum

$$\rho^{(j)}(E,r) \propto \frac{1}{\Delta E} \parallel \chi_j(E,r)\parallel^2, \tag{A3}$$

where ΔE is the level spacing at the energy E and the wavefunction $\chi_j(E,r)$ should be subjected to a proper normalisation condition.

Thus, in order to compute the LDOS (A2) we have to find the properly normalised wavefunctions $\chi_j(E,r)$ of equation (A1) and the level spacing ΔE. This task may be easily performed using another property of confinement potential: $U(r)$ is constant in the limiting regions of small and large r.

Indeed, if $U(r) \equiv U_f =$ constant in the region of $r \geqslant r_f$, then in this region equation (A1) can be solved exactly. Corresponding eigenfunctions $\chi_j(E,r)$ can be then expressed in terms of two integral constants $C_f = (C_f^{(1)}, C_f^{(2)})^T$ as

$$\chi_j(E,r) = \mathcal{W}_f(U_f,r)C_f \tag{A4}$$

with $\mathcal{W}_f(U_f,r)$ being the basic solution of equation (A1) in this region

$$\mathcal{W}_f(U_f,r) = \begin{pmatrix} J_{j-\frac{1}{2}}(q_f r) & Y_{j-\frac{1}{2}}(q_f r) \\ \mathrm{i}\tau_f J_{j+\frac{1}{2}}(q_f r) & \mathrm{i}\tau_f Y_{j+\frac{1}{2}}(q_f r) \end{pmatrix}.$$

Here, $J_{j\pm\frac{1}{2}}$ and $Y_{j\pm\frac{1}{2}}$ denote the Bessel functions of the first and second kind, respectively, $q_f = |E - U_f|$ and $\tau_f = \mathrm{sign}(E - U_f)$.

Imagine that the studied structure is entirely embedded in a very large graphene disk of radius $L \gg r_f$. From the fact that, on the one hand, the solution (A4) should hold for much of area of this disk and, on the other hand, the wave function should vanish at $r = L$ and larger distances, one can immediately deduce the level spacing

$$\Delta E = \pi/L \tag{A5}$$

and the wanted normalisation condition for $\chi_j(E,r)$:

$$\frac{4L\,\|C_f\|}{|E - U_f|} = 1. \tag{A6}$$

Further, since the confinement potential is also constant in the region of small distances, $U(r) \equiv U_i =$ constant at $r \leqslant r_i$, equation (A1) could be solved exactly in this region close to the origin and the found eigenfunctions have a simple form

$$\chi_j(E,r) = \mathcal{N}\begin{pmatrix} J_{j-\frac{1}{2}}(q_i r) \\ \mathrm{i}\tau_i J_{j+\frac{1}{2}}(q_i r) \end{pmatrix}. \tag{A7}$$

where $q_i = |E - U_i|, \tau_i = \mathrm{sign}(E - U_i)$, and $\mathcal{N}$ is the normalisation coefficient [19]. The solutions (A7) at $r = r_i$ can be in turn used as the initial values in solving the differential equation (A1).

Thus, with the initial values (A7) and the normalisation condition (A6) we can iteratively solve the differential equation (A1) to find proper wavefunctions $\chi_j(E,r)$. Obtained $\chi_j(E,r)$ and the level spacing (A5) are then inserted into (A2) to calculate the LDOS.

Once the LDOS-spectrum $\rho(E,r)$ (A2) is known, to access the resonances in it, one should calculate the TDOS which is defined by [19]:

$$\rho_T(E) = \int_0^{R_{\max}} 2\pi \mathrm{d}r\rho(E,r), \tag{A8}$$

where the integral should be cut off at some $r = R_{\max}$ which encircles the major maxima of the calculated LDOS.

In practice, given potential $U(r)$, the process of computing LDOSs and TDOSs may be schemed as

(a) Solving exactly equation (A1) in the regions $r \geqslant r_f$ and $r \leqslant r_i$, where $U(r) \equiv U_f$ and $U(r) \equiv U_i$, to find the solutions (A4) and (A7), respectively.

(b) Solving numerically equation (A1) to find the radial wavefunction $\chi_j(E,r)$, using the initial values $\chi_j(E,r)$ (A7) at $r = r_i$ and the normalisation condition (A6). Note that in the absence of an external magnetic field the energy spectra of systems under study are identical for $j > 0$ and $j < 0$ [16], so we need to consider only the case $j > 0$.

(c) Calculating the partial LDOSs $\rho^{(j)}(E,r)$ (A3) and then LDOS $\rho(E,r)$ (A2), using obtained wavefunctions $\chi_j(E,r)$ and the level spacing ΔE (A5). Reasonably, the summation over j in (A3) should be truncated at some $j_{\max}$, implying that the higher momenta do not contribute significantly to the LDOS at the energy scale of interest. The value of $j_{\max}$ should be determined for the studied sample in the way as shown in figure A1 for the sample analysed in figure 2(d) where $j_{\max}$ is taken to be $31/2$. In the same way the momentum $j_{\max}$ was determined for all the data presented in figures 4–6. For example, for LDOSs presented in figures 4 and 5, $j_{\max} = 29/2$ and $51/2$, respectively. It should be here mentioned that this way of determining $j_{\max}$ was just used by Zhao *et al* [12] in calculating LDOSs for circular graphene resonators created by the parabolic potential of $U(r) \propto r^2$. In the closely related problem of resonant scattering Masir *et al* [30] have also used the same way of determining $j_{\max}$ in calculating the total cross section for circular graphene quantum dots (CGQDs) with an impenetrable edge (it is 15 in figures 2 and 3 in this reference).

(d) Calculating the TDOS (A8), where the cut-off distance $R_{\max}$ is merely taken about 2 times of the effective radius of the studied resonator (see figures 3–5 and accompanied discussions).

The calculating method described above is in equal applied to calculate the LDOSs/TDOSs for all circular graphene junctions under study, including all types of uni-junctions (e.g. np or pp′) as well as bipolar-junctions (e.g. pnp). For each junction type the study should be carried out for many

Table B1. Partial Q_i-factors of five most profound resonances and their average Q-factor for each EWGM-spectrum presented in figures 6(a)–(c). The spectra are labelled by (si), $i = 1$–9, and the resonances in each spectrum are labelled by numbers 1–5.

	Partial quality-factors					
EWGM spectra	1	2	3	4	5	Average Q
(s1)	31.19	23.73	19.84	18.30	16.98	22.01 ± 5.72
(s2)	40.40	61.82	104.47	85.60	43.66	67.19 ± 27.51
(s3)	33.20	66.97	102.03	80.36	40.39	64.59 ± 28.40
(s4)	24.11	25.25	21.40	18.21	15.57	20.91 ± 4.03
(s5)	57.24	68.50	60.14	51.09	44.98	56.39 ± 8.94
(s6)	19.18	18.11	16.64	15.65	14.67	16.85 ± 1.82
(s7)	97.18	87.36	93.95	79.90	79.20	87.52 ± 8.09
(s8)	112.76	108.47	117.66	103.68	109.55	110.43 ± 5.19
(s9)	112.61	116.77	105.16	108.02	100.58	108.63 ± 6.31

Table B2. The same as table B1, but for the partial mode R_i-radii, their average value R and average resonance spacing Δ.

	Partial mode radii						
EWGM spectra	1	2	3	4	5	Average R (nm)	Average Δ (meV)
(s1)	22.42	21.66	21.66	21.66	21.55	21.79 ± 0.36	45.90 ± 0.736
(s2)	32.18	29.21	26.59	26.12	25.66	27.95 ± 2.73	36.04 ± 3.314
(s3)	24.39	21.98	19.82	19.47	19.14	20.96 ± 2.21	48.11 ± 4.756
(s4)	18.20	18.27	18.42	18.58	18.73	18.44 ± 0.22	54.23 ± 0.644
(s5)	14.42	14.37	14.37	14.46	14.51	14.42 ± 0.06	69.33 ± 0.293
(s6)	21.55	21.44	21.45	21.55	21.55	21.51 ± 0.06	46.49 ± 0.125
(s7)	37.63	37.63	37.95	37.63	38.28	37.82 ± 0.29	26.44 ± 0.201
(s8)	47.23	47.23	47.23	47.23	48.26	47.44 ± 0.46	21.08 ± 0.202
(s9)	67.27	66.27	67.27	67.27	67.27	67.07 ± 0.45	14.91 ± 0.101

samples with different potential parameter values, searching for the LDOSs with EWGMs. Fortunately, computations may be easily performed using standard MatLab or C++ programs.

Appendix B. Quantitative analyses of EWGMs

For each EWGM-spectrum identified we evaluated its overall characteristics, including the Q-factor, mode radius R and resonance spacing Δ. To this end, for the most profound (i)-resonances in the spectrum we evaluated the resonance energy E_i (i.e. the energy-position of resonance peak), the resonance width δE_i and the resonance spacing ΔE_i (see figure 6(d)). Obtained data are then used to determine the partial Q_i-factors and mode radii R_i for examined resonances, following the same way as that for optical WGMs (see main text). Then, from these partial Q_i-factors, R_i-radii, and ΔE_i-spacings we deduced the average values, Q, R, and Δ which characterise the studied EWGM on the whole. As an example, tables B1 and B2 respectively show in detail the Q-factors (partial and average) and the mode radii (partial and average) as well as the average resonance spacings found for the EWGM-spectra presented in figure 6(a)–(c).

Appendix C. Resonant spectra in large resonators

It should be emphasised that all the potential parameters are closely correlated with each other in affecting the resonant spectra of studied resonators. So, in response to changes of a particular potential parameter, say the effective radius L, the varying feature of resonant spectrum is essentially depending on the values of other parameters, say U_l, U_g, and α for CGNPJs. As a demonstration, figure C1 shows how the resonant spectrum of a resonator changes when only its radius varies. The data shown in figures C1(a)–(c) are for three sets of resonators, which are respectively originated from the resonators studied in figures 3–5.

In figure C1(a) the top curve is just the TDOS with EWGMs shown in figure 2(d) for the CGNPJ of radius $L = 30$ nm. With increasing the radius L to 50, then 75 and then 100 nm, keeping other parameters unchanged, the spectra in the energy region of interest show more and more resonances, which however become badly defined and less equidistant. Such the changes of spectra as L increases are more noticeable in figure C1(b) for CGPP′Js with different radii, including the CGPP′J with $L = 25$ nm studied in figure 4. In figure C1(c) for CGPNPHJs the radius L is specially increased to the value of 500 nm. There

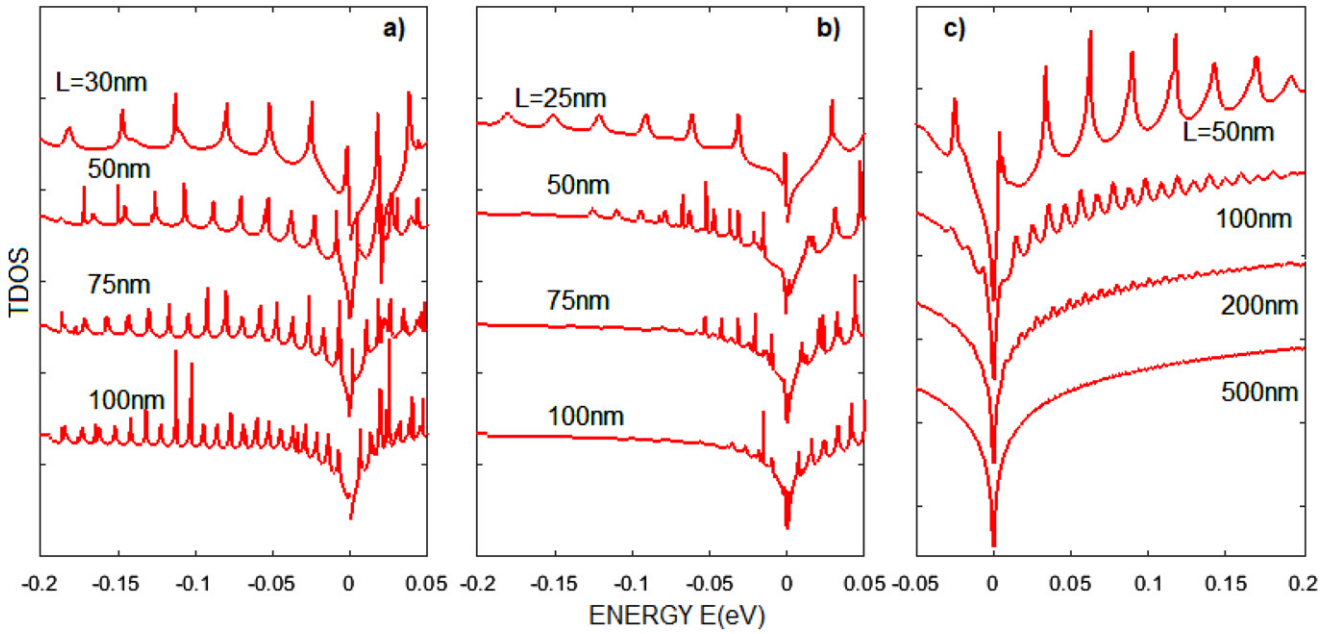

Figure C1. Changes of TDOSs (describing resonant spectra) as the resonator radius increases. The TDOSs in each box are for the resonators differentiated from each other only by the radius value (given to curves). (a) ((b) or (c)) is for CGNPJs (CGPP′Js or CGPNPHJs), where the top curve is just the TDOS presented in figure 2(d) (figures 4(c) or 5(c), respectively)

is no limiting radius of observing EWGMs that applies for all resonators. However, generally, the larger the radius L, the weaker the confinement effect and, therefore, the smaller the probability of finding EWGM-spectra. In the present study, we have examined many resonators of each junction type and recognised no resonator with $L > 100$ nm that exhibits an EWGM-spectrum. So, in combination with the studies on the size dependence of confinement effect in CGQDs, e.g. in [31], we hereby suggested that within the framework of the studied models the EWGM-spectra could be observed only in the resonators of $L \leqslant 100$ nm. Really, this is just an empirical estimation.

Here, we would like to note on a certain relation between the resonator radius and the value of $j_{\max}$ which should be used in determining LDOSs (see appendix A). For CGQDs with zigzag boundary conditions (one of wave-components is zero at the dot edge), Wunsch *et al* [32] were able to estimate the maximum value of angular momentum for the surface states, $j_{\max} \sim R/l$, where R is the dot radius and l is a length comparable to the lattice spacing. For the studied circular graphene junctions which are created by rather complicated electrostatic potentials of equation (2) or (3), $j_{\max}$ must be determined for each computed sample in the way as described in figure A1. We also noticed that $j_{\max}$ becomes larger as the resonator radius increases. However, this statement is valid only if comparisons are taken among the resonators with the same values of all potential parameters other than the radius (that varies) due to a strong correlation between these parameters and the radius in affecting resonant spectra.

ORCID iDs

V Lien Nguyen https://orcid.org/0000-0001-8696-3964

References

[1] Vahala K J 2003 Optical microcavities *Nature* **424** 839
[2] Oraevsky A N 2002 Whispering-gallery waves *Quantum Electron.* **32** 377
[3] Matsko A B and Ilchenko V S 2006 Optical resonators with whispering gallery modes I: basics *IEEE J. Sel. Top. Quantum Electron.* **12** 3
[4] Pöllinger M, O'Shea D, Warken F and Rauschenbeutel A 2009 Ultrahigh-Q tunable whispering-gallery-mode microresonator *Phys. Rev. Lett.* **103** 053901
[5] Acharyya N and Kozyreff G 2019 Large Q-factor with very small whispering-gallery-mode resonators sl *Phys. Rev. Appl.* **12** 014060
[6] Castro Neto A H, Guinea F, Peres N M R, Novoselov K S and Geim A K 2009 The electronic properties of graphene *Rev. Mod. Phys.* **81** 109
[7] Cheianov V V, Fal'ko V and Altshuler B L 2007 The focusing of electron flow and a Veselago lens in graphene p-n junctions *Science* **315** 1252
[8] Lee G H, Park G H and Lee H J 2015 Observation of negative refraction of Dirac fermions in graphene *Nat. Phys.* **11** 925
[9] Gutierrez C, Brown L, Kim C J, Park J and Pasupathy A N 2016 Klein tunneling and electron trapping in nanometre-scale graphene quantum dots *Nat. Phys.* **12** 1069
[10] Lee J *et al* 2016 Imaging elecrostatically confined Dirac fermions in graphene quantum dots *Nat. Phys.* **12** 1032
[11] Freitag N M *et al* 2016 Electrostatically confined monolayer graphene quantum dots with orbital and valley splittings *Nano Lett.* **16** 5798
[12] Zhao Y *et al* 2015 Creating and probing electron whispering-gallery modes in graphene *Science* **348** 672
[13] Ghahari F *et al* 2017 An on/off Berry phase switch in circular graphene resonators *Science* **356** 845–9
[14] Jiang Y *et al* 2017 Tuning a circular p–n junction in graphene from quantum confinement to optical guiding *Nat. Nanotechnol.* **12** 1045

[15] Ren Y N *et al* 2019 Scanning tunneling microscope characterizations of a circular graphene resonator realized with p-p′ junctions (arXiv:1908.06582) [cond-mat]
[16] Matulis A and Peeters F M 2008 Quasibound states in quantum dots in single and bilayer graphene *J. Phys.: Condens. Matter* **77** 115423
[17] Chen H Y, Apalkov V and Chakraborty T 2007 Fock-Darwin states of Dirac electrons in graphene-based artificial atoms *Phys. Rev. Lett.* **98** 186803
[18] Nguyen H C, Nguyen N T T and Nguyen V L 2016 The transfer matrix approach to circular graphene quantum dots *J. Phys.: Condens. Matter* **28** 275301
[19] Nguyen H C, Nguyen N T T and Nguyen V L 2017 On the density of states of circular graphene quantum dots *J. Phys.: Condens. Matter* **29** 405301
[20] Huard B *et al* 2007 Transport measurements across a tunable potential in graphene *Phys. Rev. Lett.* **98** 236803
[21] Sonin E B 2009 Effect of Klein tunneling on conductance and shot noise in ballistic graphene *Phys. Rev.* B **79** 195438
[22] Cabosart D, Felten A, Reckinger N, Iordanescu A, Toussaint S, Faniel S and Hackens B 2017 Recurrent quantum scars in a mesoscopic graphene ring *Nano Lett.* **17** 1344
[23] Dinh T D L, Nguyen H C and Nguyen V L 2018 Quasibound states in single-layer graphene quantum rings *J. Phys.: Condens. Matter* **30** 315501
[24] Downing C A, Stone D A and Portnoi M E 2011 Zero-energy states in graphene quantum dots and rings *Phys. Rev.* B **84** 155437
[25] Wang Y *et al* 2013 Observing atomic collapse resonances in artificial nuclei on graphene *Science* **340** 734
[26] Davies J H 1998 *The Physics of Low-Dimensional Semiconductors: An Introduction* (Cambridge: Cambridge University Press)
[27] Bardarson J H, Titov M and Brouwer P W 2009 Electrostatic confinement of electrons in an integrable graphene quantum dot *Phys. Rev. Lett.* **102** 226803
[28] Katsnelson M I, Novoselov K S and Geim A K 2006 Chiral tunnelling and the Klein paradox in graphene *Nat. Phys.* **2** 620 see also Todorovskiy *et al* 2012 *Phys. Scr.* **T146** 014010
[29] Dell'Anna L, Majari P and Setare 2018 From Klein to anti-Klein tunneling in graphene tuning the Rashba spin–orbit interaction or the bilayer coupling (arXiv:1806.06962 [cond-mat.mes-hall])
[30] Masir M R, Matulis A and Peeters F M 2011 Scattering of Dirac electrons by circular mass barriers: valley filter and resonant scattering *Phys. Rev.* B **84** 245413
[31] Ponomarenko L A *et al* 2008 Chaotic Dirac billiard in graphene quantum dots *Science* **320** 356
[32] Wunsch B, Tauber T and Guinea F 2008 Electron–electron interactions and charging effects in graphene quantum dots *Phys. Rev.* B **77** 035316